

# Simulation, Design and Fabrication of a Mach-Zehnder Interferometer

Sam Almulla

July 08, 2025

## Abstract

We present the end-to-end design, fabrication, and characterization of unbalanced silicon Mach-Zehnder interferometers (MZIs). A compact model for 500 nm x 220 nm strip waveguides was extracted from eigen-mode simulations in Lumerical MODE and imported into Lumerical INTERCONNECT to simulate the group refractive index and free-spectral range (FSR) across process corners. Six MZIs with path-length differences from 100  $\mu\text{m}$  to 200  $\mu\text{m}$  were laid out and fabricated through the NanoSOI multi-project-wafer (MPW) electron-beam process. Wafer test data was then collected and analyzed, yielding group-index and FSR values that matched simulations for five of the six devices. The exercise covered every step of the silicon photonics flow in an accessible and hands-on manner and served as a great teaching tool for engineers interested in silicon photonics.

## 1 Introduction

Silicon photonics combines the low-cost, high-volume strengths of CMOS fabs with the speed of optical devices. Since Soref & Bennett's 1987 early research on electrooptical effects in silicon [1] and the first silicon modulators of the 1990s, platforms such as standard PDKs and multi-project wafer (MPW) services [2] have enabled applications from datacom to biosensing [3]. In this report, we review the silicon photonic integrated circuit design workflow by simulating, designing, fabricating and testing simple unbalanced Mach-Zehnder Interferometers (MZIs).

## 2 Theory

Mach-Zehnder interferometers split light into two paths via beam splitters, introduce a relative phase delay and recombine to produce constructive and destructive interference at the output. Balanced MZIs (equal path lengths) convert electrically or thermally-induced phase shifts into amplitude modulation for switching and modulation applications. Unbalanced MZIs (unequal path lengths) set the free-spectral range for wavelength-sensitive applications like filtering and sensing.

An MZI consists of a Y-branch splitter connected to a Y-branch combiner by two arms. We can derive its transfer function by considering the output  $I_o$  of an incident wave  $I_i$  with an electric field  $E_i$  at the output of both of these components [4]. This transfer function is as follows (assuming negligible total loss):

$$I_o = \frac{I_i}{2} [1 + \cos(\beta_1 L_1 - \beta_2 L_2)]$$

In the case of an unbalanced MZI, we assume that the index of refraction (and propagation constant  $\beta_{1,2}$ ) between the two branches will remain the same, simplifying the equation further:

$$I_o = \frac{I_i}{2} [1 + \cos(\beta \Delta L)]$$

The period of the resulting output is determined by the Free-Spectral Range (FSR):

$$\text{FSR} = \frac{\lambda^2}{n_g \Delta L}$$

## 3 Modelling and Simulation

### 3.1 Waveguide Modeling

Waveguides act as optical wires that guide light using total internal reflection. They carry an inherent optical loss (2-3 db/cm) which must be considered when simulating our designs. There are multiple approaches to simulating waveguides in a circuit. We can use an eigenmode solver to collect  $n_{\text{eff}}/n_g$  vs  $\lambda$  data that is then used directly in our circuit simulations. Another approach is to build a compact model for the waveguide by using the same  $n_{\text{eff}}/n_g$  vs  $\lambda$  data to fit a second-order polynomial:

$$n_{\text{eff}}(\lambda) = n_1 + n_2 (\lambda - \lambda_0) + n_3 (\lambda - \lambda_0)^2.$$

Using Lumerical MODE's eigensolver we are able to simulate the effective refractive index of our waveguide across a wavelength range spanning 1500nm to 1600nm (*Fig. 1, 2*). In our simulations and final designs we use 500nm wide, 220nm high strip waveguides.

Figure 1: group refractive index versus wavelength

Figure 2: effective refractive index versus wavelength

We then fit a curve over the data (using a Lumerical MODE script [4] and obtain the following model we can use going forward:

$$n_{\text{eff}}(\lambda) = 2.44 - 1.12 (\lambda - 1.55) - 0.0341 (\lambda - 1.55)^2.$$

### 3.2 MZI Modeling

We modeled the MZI's behavior using the following circuit setup in Lumerical INTERCONNECT:

The circuit we modeled consists of a Y-branch connected to a broadband directional coupler by waveguides that use waveguide data we simulated in Lumerical MODE. We can simulate coupling in and out of the chip by connecting Fiber Grating Couplers to the input and output ports of the circuit. This allows us to model loss associated with the Fiber Grating Couplers (*Fig. 4*).

An optical network analyzer is used to sweep the wavelength from 1500nm to 1600nm and collect parametric data. For this circuit simulation, we are considering a path length difference of 100  $\mu\text{m}$  between the two waveguides. We collect data with and without the Fiber Grating Couplers attached to the circuit to observe their impact (*Fig. 5*).

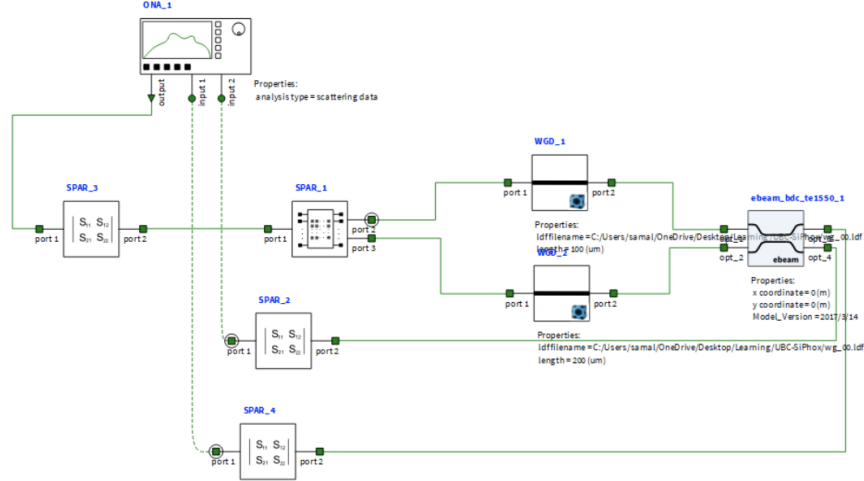


Figure 3: MZI circuit in Lumerical INTERCONNECT

Figure 4: loss versus wavelength through two grating couplers

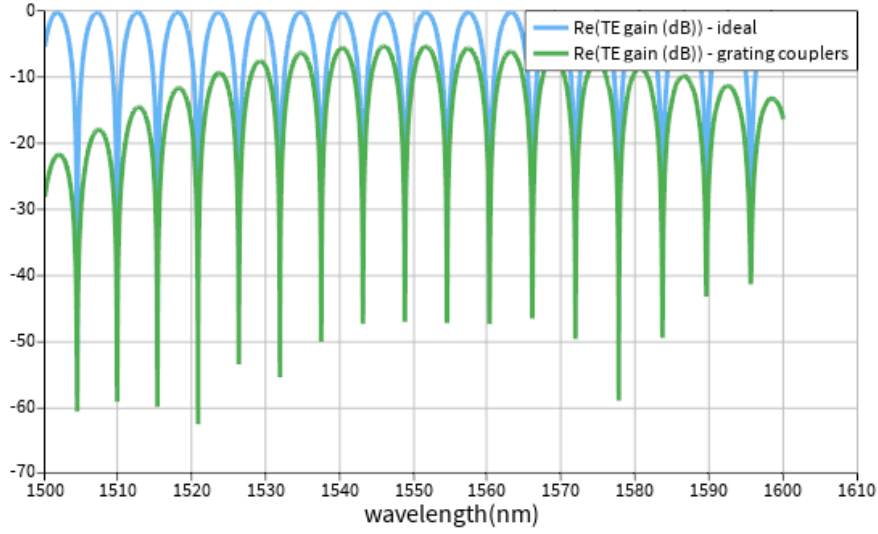


Figure 5: gain versus wavelength of the MZI circuit (with and without grating couplers)

### 3.3 Final Layout

Our final design consists of 6 different MZIs with varying path lengths from (100 to 200  $\mu\text{m}$ ) and a de-embedding structure that will allow us to compensate for grating-coupler related losses in our final analysis. We used KLayout to generate our design.

Figure 6: final KLayout design with 6 MZIs and a de-embedding structure

We consider the following devices:

Table 1: Device Configuration		
Device	Polarization	Path Length ( $\mu\text{m}$ )
CAL	—	—
MZI1	TE	100
MZI2	TE	120
MZI3	TE	140
MZI4	TE	160
MZI5	TE	180
MZI6	TE	200

By applying the FSR equation (3), we are able to calculate the predicted FSR at 1550nm across devices with different path lengths:

Table 2: Free Spectral Range (FSR) vs Path Length		
Device	Path Length ( $\mu\text{m}$ )	FSR (nm)
MZI1	100	5.752
MZI2	120	4.793
MZI3	140	4.108
MZI4	160	3.595
MZI5	180	3.195
MZI6	200	2.876

Finally, we can also simulate the FSR at varying path lengths deltas versus central wavelengths between 1500nm and 1600nm (*Fig. 6*).

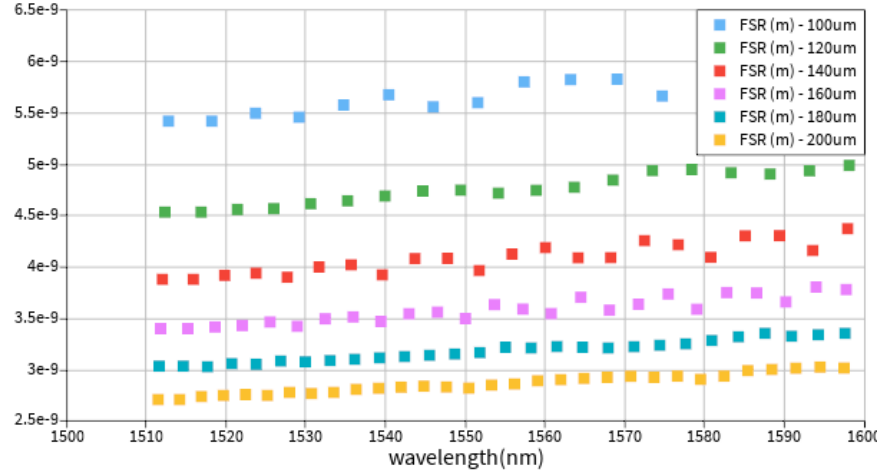


Figure 7: FSR versus wavelength across multiple different path lengths

## 4 Fabrication

### 4.1 Fabrication Process

The photonic devices were fabricated using the NanoSOI MPW fabrication process by Applied Nanotools Inc. (<http://www.appliednt.com/nanosoi>; Edmonton, Canada) which is based on direct-write 100 keV electron beam lithography technology. Silicon-on-insulator wafers of 200 mm diameter, 220 nm device thickness and 2  $\mu\text{m}$  buffer oxide thickness are used as the base material for the fabrication (Fig 8.1). The wafer was pre-diced into square substrates with dimensions of 25x25 mm, and lines were scribed into the substrate backsides to facilitate easy separation into smaller chips once fabrication was complete. After an initial wafer clean using piranha solution (3:1  $\text{H}_2\text{SO}_4\text{:H}_2\text{O}_2$ ) for 15 minutes and water/IPA rinse, hydrogen silsesquioxane (HSQ) resist was spin-coated onto the substrate and heated to evaporate the solvent (Fig 8.2). The photonic devices were patterned using a JEOL JBX-8100FS electron beam instrument at The University of British Columbia (Fig 8.3). The exposure dosage of the design was corrected for proximity effects that result from the backscatter of electrons from exposure of nearby features. Shape writing order was optimized for efficient patterning and minimal beam drift. After the e-beam exposure and subsequent development with a tetramethylammonium sulfate (TMAH) solution (Fig 8.4), the devices were inspected optically for residues and/or defects. The chips were then mounted on a 4" handle wafer and underwent an anisotropic ICP-RIE etch process using chlorine after qualification of the etch rate (Fig 8.5). The resist was removed from the surface of the devices using a 10:1 buffer oxide wet etch (Fig 8.6), and the devices were inspected using a scanning electron microscope (SEM) to verify patterning and etch quality. A 2.2  $\mu\text{m}$  oxide cladding was deposited using a plasma-enhanced chemical vapour deposition (PECVD) process based on tetraethyl orthosilicate (TEOS) at 300°C (Fig 8.7). Reflectometry measurements were performed throughout the process to verify the device layer, buffer oxide and cladding thicknesses before delivery.

Figure 8: waveguide fabrication process [5]

### 4.2 Manufacturing Variability

When simulating devices, we must take into account manufacturing variability. In order to account for it in our simulations, we apply a corner analysis to simulate our devices across 4 different process variations in the waveguide dimensions.

In order to do this, we rerun the Lumerical MODE simulations for each corner case (plotted along with the ideal case). Using a modified version of the provided waveguide Lumerical MODE  $n_{\text{eff}}$  sweep script, we simulate effective index and group index versus wavelength and extract the compact model from our simulated results using MATLAB.

Figure 9: group refractive index versus wavelength

Figure 10: effective refractive index versus wavelength

We are able to then calculate the predicted FSR for each of our MZI devices with varying path lengths by using the FSR equation defined in Theory section (3).

Table 3: Corner Analysis Results

Device	Path Length (um)	Waveguide Width (nm)	Si Thickness (nm)	$n_g$	FSR (nm)
MZI1	100	470	215.3	4.226	5.685
MZI1	100	530	215.3	4.125	5.824
MZI1	100	470	223.1	4.242	5.664
MZI1	100	530	223.1	4.139	5.805
MZI1	100	500	220.0	4.177	5.752
MZI2	120	470	215.3	4.226	4.738
MZI2	120	530	215.3	4.125	4.853
MZI2	120	470	223.1	4.242	4.720
MZI2	120	530	223.1	4.139	4.837
MZI2	120	500	220.0	4.177	4.793
MZI3	140	470	215.3	4.226	4.061
MZI3	140	530	215.3	4.125	4.160
MZI3	140	470	223.1	4.242	4.046
MZI3	140	530	223.1	4.139	4.146
MZI3	140	500	220.0	4.177	4.108
MZI4	160	470	215.3	4.226	3.553
MZI4	160	530	215.3	4.125	3.640
MZI4	160	470	223.1	4.242	3.540
MZI4	160	530	223.1	4.139	3.628
MZI4	160	500	220.0	4.177	3.595
MZI5	180	470	215.3	4.226	3.159
MZI5	180	530	215.3	4.125	3.236
MZI5	180	470	223.1	4.242	3.147
MZI5	180	530	223.1	4.139	3.225
MZI5	180	500	220.0	4.177	3.195
MZI6	200	470	215.3	4.226	2.843
MZI6	200	530	215.3	4.125	2.912
MZI6	200	470	223.1	4.242	2.832
MZI6	200	530	223.1	4.139	2.902
MZI6	200	500	220.0	4.177	2.876

## 5 Experimental Data

To characterize the devices, a custom-built automated test setup [4]; [6] with automated control software written in Python was used [7]. An Agilent 81600B tunable laser was used as the input source and Agilent 81635A optical power sensors as the output detectors. The wavelength was swept from 1500 to 1600 nm in 10 pm steps. A polarization maintaining (PM) fibre was used to maintain the polarization state of the light, to couple the TE polarization into the grating couplers [8]. A 90° rotation was used to inject light into the TM grating couplers [8]. A polarization maintaining fibre array was used to couple light in/out of the chip [9].

We collected transmission data for the 7 devices described above. We plot the raw data for MZI6 (200  $\mu\text{m}$  path length) and the de-noising structure (CAL).

Figure 11: measured insertion-loss of the calibration loopback

Figure 12: measured transmission spectrum of MZI6

## 6 Analysis

**TODO:** Describe how we extract FSR and derive  $n_g$

**TODO:** Compare to Corner Analysis

## 7 Conclusion

This work demonstrated the complete silicon-photonics design cycle for an unbalanced Mach-Zehnder interferometer (MZI). Starting from eigen-mode simulations in Lumerical MODE, we generated a compact waveguide model and calculated the group and effective indices of the 500 nm x 220 nm waveguide used in our designs. We then fed that model into Lumerical INTERCONNECT to simulate the MZI, folding in grating-coupler insertion loss and predicting the transmission spectra and FSR for multiple process corners. We repeated the waveguide and circuit simulations for different process corners. Next, we laid out six MZI devices with varying path lengths and a loopback structure for de-noising. After fabricating the devices using the NanoSOI MPW electron-beam fabrication process, automated wafer-scale measurements were performed. We analyzed the results by applying a least-squares curve fit to extract the  $n_g$  and FSR parameters for our measured transmission data. Apart from one stubborn device (MZI2), the measurement data agreed with our corner analysis and fit within our predictions.

## 8 Acknowledgements

We acknowledge the edX UBCx Phot1x Silicon Photonics Design, Fabrication and Data Analysis course, which is supported by the Natural Sciences and Engineering Research Council of Canada (NSERC) Silicon Electronic-Photonic Integrated Circuits (SiEPIC) Program. The devices were fabricated by Richard Bojko at the University of Washington Washington Nanofabrication Facility, part of the National Science Foundation's National Nanotechnology Infrastructure Network (NNIN), and Cameron Horvath at Applied Nanotools, Inc. Omid Esmaeeli performed the measurements at The University of British Columbia. We acknowledge Lumerical Solutions, Inc., Mathworks, Mentor Graphics, Python, and KLayout for the design software.

## References

1. Soref R, Bennett B (1987) Electrooptical effects in silicon. IEEE Journal of Quantum Electronics 23: <https://doi.org/10.1109/jqe.1987.1073206>
2. Siew SY, Li B, Gao F, et al. (2021) Review of Silicon Photonics Technology and Platform Development. Journal of Lightwave Technology 39: <https://doi.org/10.1109/jlt.2021.3066203>
3. Thomson D, Zilkie A, Bowers JE, et al. (2016) Roadmap on silicon photonics. Journal of Optics 18: <https://doi.org/10.1088/2040-8978/18/7/073003>
4. Chrostowski L, Hochberg M (2015) Silicon Photonics Design. Cambridge University Press (CUP)
5. Chrostowski L, Bojko R (2015) Waveguide Fabrication Steps using Electron Beam Lithography
6. <http://mapleleafphotonics.com>, Maple Leaf Photonics, Seattle WA, USA
7. <http://siepic.ubc.ca/probestation>, using Python code developed by Michael Caverley
8. Wang Y, Wang X, Flueckiger J, et al. (2014) Focusing sub-wavelength grating couplers with low back reflections for rapid prototyping of silicon photonic circuits. Optics Express 22: <https://doi.org/10.1364/oe.22.020652>

9. [www.plcconnections.com](http://www.plcconnections.com), PLC Connections, Columbus OH, USA